Particle-rotor model calculations of superdeformed bands in $A = 150$ and 190 regions

M. Saha Sarkar*

Saha Institute of Nuclear Physics, 1/AF Bidhan Nagar, Calcutta 700064, India

Quite a few superdeformed bands in the mass regions of 150 as well as 190, having different trends in the dynamic moments of inertia with increasing angular momentum, are studied in a simple version of the particle-rotor model. Transition energies, dynamic, and kinematic moments of inertia have been calculated. A reasonably good agreement with the experimental data justifies the application of this version of the model in the new regime of nuclear structure. Electromagnetic moments calculated within the same model also agree with the experimental results. The role of high-j intruder orbitals in the structure of the superdeformed bands in both the regions has been reinvestigated. [S0556-2813(99)01412-0]

PACS number(s): 21.10.Re, 23.20.Lv, 21.60.Ev, 27.60.+j

I. INTRODUCTION

Recently, the study of superdeformation [1–9] is one of the most exciting areas in nuclear physics. Numerous superdeformed (SD) bands have been observed in various mass regions, e.g., $A = 80$, 130, 150, and 190. They are associated with extremely large quadrupole deformation (β). Typical β's observed in these bands in the above-mentioned mass regions are 0.50, 0.40, 0.60, and 0.47, respectively. Study of these bands are interesting both theoretically and experimentally.

It is essential that the existing standard models which are quite successful in explaining the normally deformed nuclei should also be applied in this new domain of nuclear structure. Numerous attempts [1] have been undertaken in the last decade since the experimental observation of superdeformation in ^{152}Dy [3]. Many interesting and new conclusions have been drawn based on these studies. But there are still many questions that need to be answered.

The SD bands observed in various mass regions have their own characteristic features. The differences between the SD bands in various mass regions are manifested through the behavior of the dynamical moment of inertia $\mathfrak{I}^{(2)}$. For example, most SD bands in the $A = 190$ region exhibit the same smooth increasing trend in $\mathfrak{I}^{(2)}$ with increasing angular frequency [7,8], while the $\mathfrak{I}^{(2)}$ patterns near $A = 150$ show different variations which have been shown to be a characteristic fingerprint of active intruder orbital under consideration. The rise in $\mathfrak{I}^{(2)}$ in $A = 190$ has been suggested to rise mainly from the gradual alignment of the quasiparticles in high-N intruder orbitals and from the gradual disappearance of pairing correlation with the collective rotation.

It is, therefore, interesting and challenging to try to study and explain the different trends of $\mathfrak{I}^{(2)}$ in SD bands in the two mass regions using the same formalism.

The particle-rotor model (PRM) is one of the most useful [4–6,9–14] methods for studying the SD bands [4–6,9]. This model is conceptually simple, computationally easy to handle and thus extremely suitable for a systematic study of a particular feature in a wide mass region.

So with this in view, the superdeformed band structures in several odd-proton and odd-neutron nuclei in the mass 150 and 190 regions are calculated in a version of PRM [10,12,13] and compared with the available experimental data [1] in the present work. Calculations are done in $^{193,195}_{81}$Tl [1], $^{191,193,195}_{80}$Hg [1,16], $^{153,155}_{66}$Dy [1,17], $^{151}_{65}$Tb [1], and $^{147}_{64}$Gd [18]. The role of high-j intruder orbitals in the structure of the superdeformed bands in both the regions has been reinvestigated to explain the difference in the variation of $\mathfrak{I}^{(2)}$ with spin.

II. MODEL

A. Formalism

The model is based on the assumption that the nucleus under consideration is axially symmetric. In this model, the motion of an unpaired quasiparticle in a Nilsson deformed orbit is coupled to the rotational motion of the core through Coriolis interaction. We have used a version [10] of the PRM in which the experimental core energies can be fed directly as input parameters. The advantage of using this particular version will be discussed in detail in the next section.

The Hamiltonian of the odd-A system can be written as

$$H = H^0_{qp} + c\mathbf{R} \cdot \mathbf{j} + E_c(R). \tag{1}$$

The first term is the Hamiltonian of a single quasiparticle and is given by

$$H^0_{qp} = \sum_K E_K a^\dagger_K a_K, \tag{2}$$

with

$$E_K = \sqrt{(\epsilon_K - \lambda)^2 + \Delta^2}, \tag{3}$$

where ϵ_K is the energy of a single particle moving in a standard axially symmetric Nilsson potential. The pairing gap and the Fermi level are represented by Δ and λ, respectively.

*Electronic address: mss@anp.saha.ernet.in

The last term, $E_c(R)$, represents the collective part of the Hamiltonian, whereas the middle term, originally introduced by Neergärd [19], describes the rotational dependence of the interaction between the core and the quasiparticle. The coefficient c is defined [10] in terms of the core moment of inertia corresponding to the lowest 2^+ state in the rotational band and another parameter α. For a constant moment of inertia, α is identical to the usual Coriolis attenuation factor. Moreover, it can be shown that introduction of the $c\mathbf{R}\cdot\mathbf{j}$ term in the Hamiltonian effectively reduces the recoil energy if there is attenuation of the Coriolis matrix elements. In the limit of very small attenuation ($\alpha \simeq 1$), this interaction term loses its significance. It can be shown [10] that, in the present formalism, the Coriolis attenuation factor will, in general, be a function of the angular momentum (I) of the excited state.

The basis states are usually taken in the form

$$|IMK\rangle = [(2I+1)/8\pi^2]^{1/2}$$
$$\times [\mathcal{D}^I_{MK}\chi_K + (-)^{I-1/2}\mathcal{D}^I_{M,-K}\chi_{-K}]/\sqrt{2}. \quad (4)$$

Here χ_K represents the Nilsson single-particle states which can be expanded into eigenstates of j^2,

$$\chi_K = \sum_j C_{jK}|jK\rangle. \quad (5)$$

However, we have to transform the basis into a representation with sharp R and j to calculate the R-dependent terms in the Hamiltonian [10]. It can be shown that in this representation, the diagonal terms of the Hamiltonian for a rotational band built on a Nilsson orbital χ_K are given by

$$E_I = E_K + 2\sum_j \sum_R |C_{jK}|^2 \begin{bmatrix} j & I & R \\ K & -K & 0 \end{bmatrix}^2 |E_c(R)| \quad (6)$$

for α (Coriolis attenuation factor) = 1.0.

The total Hamiltonian [Eq. (1)] is then diagonalized, giving the energy eigenvalues and the wave functions of the final states $|IM\rangle$ in terms of the Coriolis mixing amplitudes f_{IK} and the basis states $|IMK\rangle$:

$$|IM\rangle = \sum_K f_{IK}|IMK\rangle. \quad (7)$$

In order to identify the rotational composition of the final state $|IM\rangle$, these states are expanded in terms of states with sharp R and j [20]:

$$|IM\rangle = \sum_{jR} \sum_K f_{IK}\alpha_{jR}^{(K)}|IMjR\rangle, \quad (8)$$

where

$$\alpha_{jR}^{(K)} = \sqrt{2}\begin{bmatrix} I & j & R \\ K & -K & 0 \end{bmatrix}(-1)^{j-K}C_{jK}. \quad (9)$$

So to calculate a state with total angular momentum I, where the single-particle angular momentum involved is j (say), the experimental core energies required will be given by the following range of R values:

$$R_{\max} = I + j,$$

$$R_{\min} = I - j. \quad (10)$$

B. Parameter choice

There are several parameters involved in the PRM calculations. To reduce arbitrariness in calculations due to the involvement of these parameters, we have tried to fix as many of them as possible either from experimental observable or from previous calculations. The single-particle Nilsson parameters μ and κ, in each individual nucleus have been deduced from the prescription of Nilsson *et al.* [21]. The deformation parameter δ ($=0.95\beta$) has been kept fixed for a particular mass region ($\delta = 0.475$ for $A = 190$ and 0.57 for $A = 150$). These values have been adopted from systematics and estimations of the previous authors [1]. The Fermi levels have been chosen according to the suggestions of previous particle rotor model (PRM)–cranked shell model (CSM) calculations in the $A = 190$ region [4,16]. In the $A = 150$ region, the SD bands are $\Delta I = 2$ bands. So considering them as ''decoupled'' bands, we have fixed the Fermi level λ around $K = 1/2$ for all these nuclei.

The main problem lies in the choices of pairing gap parameter, attenuation factor, and the low spin members of the SD band of the core. Their choices will be now discussed one by one.

First, we consider the pairing gap parameter and attenuation coefficient. Normally, this gap is calculated from odd-even mass difference (Δ_{o-e}) [22] for the low spin states in normally deformed nuclei. In the present case, the nuclei are superdeformed and for the $A = 150$ region, the spins involved are quite high (around 20–50 $\hbar$). Moreover, it is already well established [8] that for the SD bands, pairing gaps have completely different values, appreciably reduced with respect to odd-even mass differences.

Now, our earlier investigations [11,12] show that in the PRM calculations choices of pairing gap and attenuation factor are inter-related, due to the following reasons. In calculation of Coriolis mixed wave functions, two factors are important: (i) the strength of the interaction and (ii) the energy spacings among the quasiparticle states which are used as basis states. Both these factors depend on the pairing gap. The strength of the interaction depends inversely on the moment of inertia which in turn is a function of strength of the pairing interaction. The energy spacings between the quasiparticle states are also very sensitive to the change in the pairing gap. The larger the gap, the smaller the spacing, and the quasiparticle states are more bunched. The moment of inertia is usually taken from the experimental data. So any inaccuracy in the spacings among the quasiparticle states due to improper choice of pairing gap parameter is effectively taken into account through adjustment of attenuation factor. In this sense PRM fails to throw any light on the change of

pairing gap with increasing spin and/or increasing deformation. It has been shown [11,12] that the effect of a reduced pairing gap can be generated by using a normal pairing gap and a large attenuation of the Coriolis term or vice versa in the PRM calculation.

So we have adopted two different approaches to account for the reduction in pairing in SD bands. We have either used fixed pairing gap from odd-even mass difference (which corresponds to the full strength of pairing) and adjusted the attenuation coefficient to an appropriate value so that the pairing reduction is simulated, or have varied both the attenuation coefficient and the pairing gap to reproduce experimental spectra. In the second situation it has been seen that for $\Delta \simeq 0.2-0.4$, the experimental spectra is reproduced for a ''normal'' (as seen from previous calculations in normally deformed nuclei in the rare-earth region [11]) value of attenuation. For our convenience and to reduce arbitrariness in our calculations, we preferred to fix the pairing gap to Δ_{o-e} in most of the cases and adjusted the attenuation coefficient only to reproduce the experimental spectra.

Finally, $E_c(R)$, the collective part of the Hamiltonian, i.e., the rotating core excitation spectrum has to be supplied. SD nuclei are extremely good rotors with a nearly constant moment of inertia (m.i.), so a constant m.i. for the core may be a good approximation. Therefore, we tried a version of PRM [11], where the rotational core is assumed to have a constant moment of inertia (CMI). We used this version to calculate the lowest SD band of ^{193}Tl. The core m.i. has been estimated from the three lowest transitions of the superdeformed band of the even-even nucleus (^{192}Hg) (Table I). The results are shown in Table II, column 3 (CMI). The calculated excitation energies deviate to a great extent from the experimental values as one goes to higher spin states. Next we opted for a VMI (variable moment of inertia) core (Table II, column 4) [14], and the agreement worsened as expected. Usually this particular version of PRM with VMI incorporated in it, works best in the transitional region [14,15]. Another way to generate the core would have been to use a two-parameter formula, where the parameters are estimated by fitting the γ-transition energies of the core [4]. As an easier alternative, we adopted the present version of PRM, where the experimental core energies can be directly used as input parameters.

The choice of the core needs a special mention unlike in the usual cases of such calculations [12,13]. We have fed in the experimental excitation energies of the underlying core as input parameters. But the core energies are not taken from the yrast bands of the neighboring even-even nucleus, they are taken from the lowest (unless mentioned otherwise) superdeformed band existing in the neighboring even-even nucleus. Now the problem arises at this point. The superdeformed bands usually start at $I \gg 0$ in the $A \simeq 150$ region. They originate at spin $\simeq 20$. In the Hg region, the minimum spin in a superdeformed band is 8–10. Now as already mentioned, the coefficient c of the $\mathbf{R} \cdot \mathbf{j}$ term in Eq. (1) is defined in terms of the core moment of inertia corresponding to the lowest 2^+ state in the core spectrum. Moreover, according to Eq. (10) the minimum core state required to generate the minimum angular momentum (I) state of the neighboring

TABLE I. Representative values of $\mathcal{A}$ ($=\hbar^2/2\mathfrak{J}$) for each of the lowest few transitions (E_γ in keV) of superdeformed bands of some even-even isotopes. R.m.s. deviations (σ) in $\mathcal{A}$ calculated are also shown.

Isotope	$I_i^+ \rightarrow I_f^+$	E_γ	$\mathcal{A}$	$\langle \mathcal{A} \rangle$	σ
^{192}Hg	$10 \rightarrow 8$	214	5.63		
	$12 \rightarrow 10$	258	5.61	5.60	0.03
	$14 \rightarrow 12$	300	5.56		
^{192}Hg [a]	$8 \rightarrow 6$	214	7.13		
	$10 \rightarrow 8$	258	6.79	6.81	0.25
	$12 \rightarrow 10$	300	6.52		
^{194}Hg	$10 \rightarrow 8$	212	5.58		
	$12 \rightarrow 10$	254	5.52	5.53	0.04
	$14 \rightarrow 12$	296	5.48		
^{190}Hg	$14 \rightarrow 12$	317	5.87		
	$16 \rightarrow 14$	360	5.80	5.77	0.07
	$18 \rightarrow 16$	402	5.74		
	$20 \rightarrow 18$	443	5.68		
^{152}Dy	$26 \rightarrow 24$	602	5.90		
	$28 \rightarrow 26$	648	5.89		
	$30 \rightarrow 28$	693	5.87		
	$32 \rightarrow 30$	738	5.86	5.87	0.02
	$34 \rightarrow 32$	784	5.85		
	$36 \rightarrow 34$	830	5.85		
^{146}Gd [b]	$35 \rightarrow 33$	826	5.99		
	$37 \rightarrow 35$	878	6.01		
	$39 \rightarrow 37$	931	6.04	6.03	0.03
	$41 \rightarrow 39$	983	6.07		
^{146}Gd [c]	$32 \rightarrow 30$	826	6.56		
	$34 \rightarrow 32$	878	6.55		
	$36 \rightarrow 34$	931	6.56	6.55	0.005
	$48 \rightarrow 36$	983	6.55		
^{150}Gd [b]	$34 \rightarrow 32$	815	6.08		
	$36 \rightarrow 34$	849	5.98		
	$38 \rightarrow 36$	888	5.92	5.92	0.09
	$40 \rightarrow 38$	929	5.88		
	$42 \rightarrow 40$	971	5.85		
	$44 \rightarrow 42$	1013	5.82		
^{150}Gd [c]	$48 \rightarrow 46$	815	4.29		
	$50 \rightarrow 48$	849	4.29		
	$52 \rightarrow 50$	888	4.31	4.33	0.04
	$54 \rightarrow 52$	929	4.34		
	$56 \rightarrow 54$	971	4.37		
	$58 \rightarrow 56$	1013	4.40		

[a]Lowest spin changed by 2 as discussed in Sec. II B.
[b]Spin mentioned in Nuclear Data Sheets [1] [NDS].
[c]Spin predicted by Eq. (11).

TABLE II. Comparison of calculated gamma transition energies [$E_\gamma(I) = E(I) - E(I-2)$ in keV] of ^{193}Tl using different versions of PRM as discussed in the text.

I	$E_\gamma^{\rm expt}(I)$	$E_\gamma^{\rm calc}(I)$		
		CMI [11]	VMI [14]	Present version [12]
10.5	206.6	206.7	205.1	206.7
11.5	227.2	227.6	224.0	226.8
12.5	247.4	248.4	239.9	247.3
13.5	267.4	269.4	256.2	267.8
14.5	287.6	290.2	270.0	287.8
15.5	308.6	311.5	284.3	308.6
16.5	327.4	332.2	296.4	328.1
17.5	348.0	353.7	309.3	348.2
18.5	366.3	374.4	320.0	367.3
19.5	387.1	396.1	331.7	387.1
20.5	405.1	416.7	341.4	405.8
21.5	425.3	438.7	352.1	425.3
22.5	442.9	459.2	360.9	443.5
23.5	463.7	481.5	370.8	462.9
24.5	479.7	501.8	378.9	480.5
25.5	501.1	524.4	388.2	499.6
26.5	516.1	544.6	395.7	516.8
27.5	537.5	567.6	404.4	535.3
28.5	551.7	587.5	411.4	552.1
29.5	573.4	610.8	419.6	570.5
30.5	586.5	630.5	426.2	586.8
31.5	608.8	654.3	434.0	604.8
32.5	620.3	673.6	440.2	620.7
33.5	643.8	697.8	447.6	638.5
34.5	653.6	716.8	453.5	654.0
35.5	678.7	741.4	460.6	671.4
36.5	686.1	760.1	466.2	686.5
37.5	713.2	785.2	473.0	703.6
38.5	718.7	803.5	478.3	718.4
39.5	747.5	829.0	484.8	735.5

TABLE III. Table of minimum core angular momentum $R_{\rm min}$ [$R_{\rm min} = I_{\rm min} - j$, Eq. (10)] needed to generate the lowest spin [1] ($I_{\rm min}^{\rm NDS}$) state in superdeformed bands in various odd-A isotopes. Spin value of the lowest SD core state as mentioned in the Nuclear Data Sheets (NDS) [1] ($R^{\rm NDS}$) is also shown in the table. j indicates the single-particle intruder angular momentum, which couples with the core.

Isotope	$I_{\rm min}^{\rm NDS}$	j	$R_{\rm min}$	$R^{\rm NDS}$	Core
$^{193}_{81}$Tl	8.5	$i_{13/2}$	2	8	^{192}Hg
$^{195}_{81}$Tl	5.5	$i_{13/2}$	0	8	^{194}Hg
$^{193}_{80}$Hg	9.5	$j_{15/2}$	2	8	^{192}Hg
$^{191}_{80}$Hg	15.5	$j_{15/2}$	8	12	^{190}Hg
$^{153}_{66}$Dy	31.5	$j_{15/2}$	24	24	^{152}Dy
$^{155}_{66}$Dy	40.5	$i_{13/2}$	34	28	^{154}Dy
$^{147}_{64}$Gd	27.5	$j_{15/2}$	20	30	SD-1 ^{146}Gd
		$i_{13/2}$	21	32	SD-2 ^{146}Gd
$^{151}_{65}$Tb (SD-1)	28.5	$j_{15/2}$	22	24	^{152}Dy
(SD-2)	24.5	$i_{13/2}$	18		
$^{195}_{80}$Hg	11.5	$i_{13/2}$	5	8	^{194}Hg
		$j_{15/2}$	4		

mation is able to generate the odd-A SD spectrum.

We have used the simple, familiar formula $E_I = (\hbar^2/2\mathfrak{J})I(I+1)$ to extrapolate the experimentally obtained superdeformed band in an even-even nuclei to lower spins as required by the present formalism. The lowest 4 or 5 transitions of a superdeformed band have been fitted and the corresponding values of $\mathcal{A}(=\hbar^2/2\mathfrak{J})$ are determined (Table I). From the values of the deviation calculated, it is evident that the moments of inertia are nearly constant. An average value of $\mathcal{A}$ is chosen and used for extrapolating the energies of the lower spin states. The spin assignments of SD bands are usually accurate to a few $\hbar$ [2,23]. So we have tested the effect of such uncertainties on the value of moment of inertia determined. The spin value of the lowest member of a SD band has been changed by $2\hbar$, and then the values of $\mathcal{A}$ are calculated (e.g., for ^{192}Hg in Table I, $I_{\rm min}=8$ [1] has been changed to 6). It is seen from the table that such a change disturbs the constancy in the value of $\mathcal{A}$ and increases the value of deviation by an order of magnitude. Therefore, we thought that this simple method may be convenient for a first-hand estimate of the minimum spin ($I_{\rm min}$) of a SD band. The ratio between two consecutive gamma rays, $E_{\gamma_1}(I_{\rm min}+4 \rightarrow I_{\rm min}+2)$ and $E_{\gamma_2}(I_{\rm min}+2 \rightarrow I_{\rm min})$, connecting the lowest spin state ($I_{\rm min}$) and two immediate upper spin states ($I_{\rm min}+2$ and $I_{\rm min}+4$) is given by

$$\frac{E_{\gamma_1}}{E_{\gamma_2}} = \frac{4I_{\rm min}+14}{4I_{\rm min}+6},$$

$$I_{\rm min} = \left[\frac{8 \times E_{\gamma_1}}{E_{\gamma_2} - E_{\gamma_1}} - 6 \right] \Big/ 4. \qquad (11)$$

odd-A nucleus is given in Table III. This table clearly shows that in most of the cases the spin of the superdeformed core state required is lower than the spin of the lowest superdeformed core state obtained experimentally (as quoted in Ref. [1]). So as a first approximation, we have made a very simplistic assumption and generated the lower states using the information of the existing states. As is well known, the superdeformed bands possess extremely large deformation. For such a well-deformed band, the moment of inertia is nearly equal to the rigid-body value and it is nearly constant. We assumed the SD bands of the core to have an exactly constant moment of inertia in the extrapolation region. This is the simplest way of generating the core energies below the experimentally obtained states. We have already seen that the constant moment of inertia for the core is not a good assumption for SD bands. We, therefore, now want to test whether the constant moment of inertia for the lowest part of the core SD band and experimental energies for the rest of the band can reproduce the SD states of the nearest odd-A nucleus. We want to see how far this uninteresting approxi-

TABLE IV. Comparison of minimum spins (I_{min}^{calc}) of different SD bands in various isotopes calculated by Eq. (11) and corresponding value (I_{min}^{NDS}) as quoted in [1]. The two consecutive gamma energies (in keV) used as E_{γ_1} and E_{γ_2} in the above equation are also mentioned.

Isotope	I_{min}^{NDS}	I_{min}^{calc}	E_{γ_1}	E_{γ_2}
	Odd-*A* Isotopes:			
^{193}Tl	8.5	8.8	207	247
^{195}Tl	5.5	5.4	146	188
^{191}Hg (SD-1)	15.5	13.7	311	352
^{191}Hg (SD-2)	10.5	10.3	252	293
^{193}Hg	9.5	9.9	233	274
^{195}Hg	14.5	15.7	334	373
^{153}Dy	31.5	30.5	721	766
^{155}Dy		40.9	910	952
^{147}Gd	27.5	27.4	697	745
^{151}Tb(SD-1)	24.5	25.7	602	646
	Even-*A* Isotopes:			
^{190}Hg	12	13.2	317	360
^{192}Hg (SD-1)	10	10.3	241	282
^{192}Hg (SD-2)	8	8.2	214	258
^{194}Hg	8	8.6	212	254
^{152}Dy	24	24.7	602	648
^{154}Dy		28.4	749	702
^{146}Gd (SD-1)	33	30.3	826	878
^{146}Gd (SD-2)	32	30.1	806	857
^{150}Tb	24	22.4	597	647
^{150}Gd	32	46.4	815	849

We used the above equation and estimated the minimum spin values for a number of SD bands in different nuclei. They are tabulated in Table IV. It can be easily seen that except for ^{150}Gd, the minimum spin predicted by this simple procedure is very close to that quoted in the published compilation [1]. This result has encouraged us to assign I_{min} value to the SD bands in ^{154,155}Dy. These values have been used later in our PRM calculations for ^{155}Dy.

The dynamical and kinematic moments of inertia of the bands have been calculated using the following relations [1]:

$$\mathfrak{J}^{(1)}(J) = \frac{4J}{E_\gamma[(J+2) \to J] + E_\gamma[J \to (J-2)]} \hbar^2 \, \text{MeV}^{-1},$$

$$\mathfrak{J}^{(2)}(J) = \frac{4}{E_\gamma[(J+2) \to J] - E_\gamma[J \to (J-2)]} \hbar^2 \, \text{MeV}^{-1}.$$

$$(12)$$

The lowest quasiparticle states originating primarily from the intruder orbital in the relevant shell are usually included in the calculation.

We have calculated the energy spectra and electromagnetic properties of superdeformed bands in $A = 150$ and 190 regions in both odd neutron and proton nuclei using the above model. Transition probabilities and electromagnetic
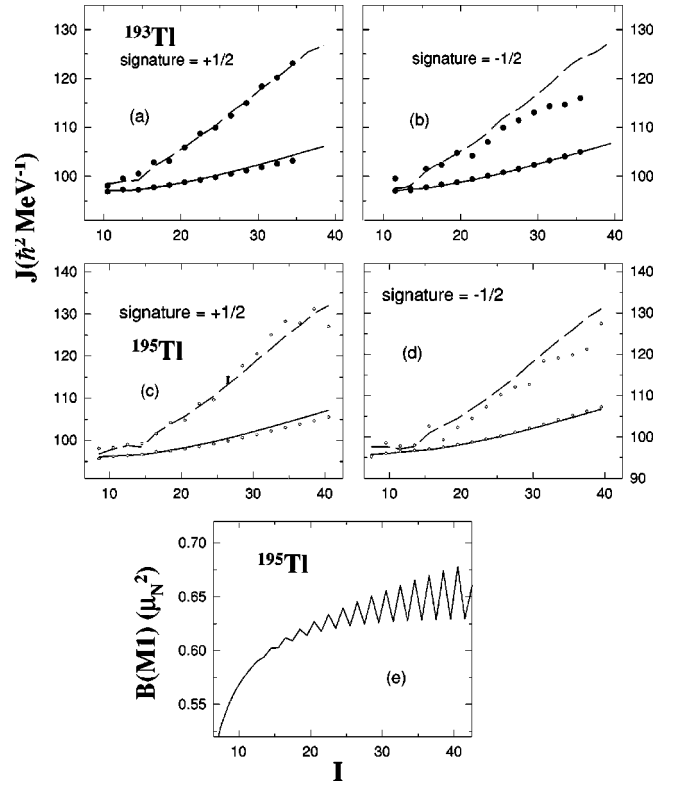
FIG. 1. (a), (b), (c), and (d) Comparison between theoretical and experimental kinematic and dynamic moments of inertia $\mathfrak{J}^{(1)}$ and $\mathfrak{J}^{(2)}$ for (a) and (c) $+1/2$ signature states, (b) and (d) $-1/2$ signature states of ^{193}Tl and ^{195}Tl, respectively. The experimental data are marked by symbols. The corresponding theoretical points are joined by lines, continuous for $\mathfrak{J}^{(1)}$ and dashed for $\mathfrak{J}^{(2)}$. (e) Calculated $B(M1; I \to I-1)$ values of the SD states in ^{195}Tl.

moments of odd-proton nucleus ^{195}Tl are calculated with $g_{lp} = 1$, $(g_s)_{eff} = 0.7g_s = 3.91$, $g_R = Z/A = 0.40$, and $(e_p)_{eff} = 0.05$ [6]. The intrinsic quadrupole moment ($Q_o = 19 \, eb$) used in the calculation is from Ref. [24]. The experimental transition energies are used in the calculation of transition probabilities. The detailed structures of the wave functions of the superdeformed states in these two mass regions are compared with wave functions of normally deformed states. This comparison is useful for understanding the difference in structure between a normal deformed and a superdeformed state, as well as the difference between superdeformed states in two different mass regions.

III. RESULTS AND DISCUSSIONS

A. Comparison of the structure of SD bands in $A = 150$ and 190 mass regions

The SD bands observed in mass regions $A \simeq 150$ and 190, have their own characteristic features. The differences between the SD bands in these two mass regions are manifested through the behavior of dynamical moments of inertia $\mathfrak{J}^{(2)}$. Most SD bands in $A = 190$ region exhibit an increasing trend in $\mathfrak{J}^{(2)}$ with increasing angular frequency (Figs. 1–3). This behavior has been explained in terms of high-j alignment and Coriolis antipairing effects [23], while the $\mathfrak{J}^{(2)}$ for the
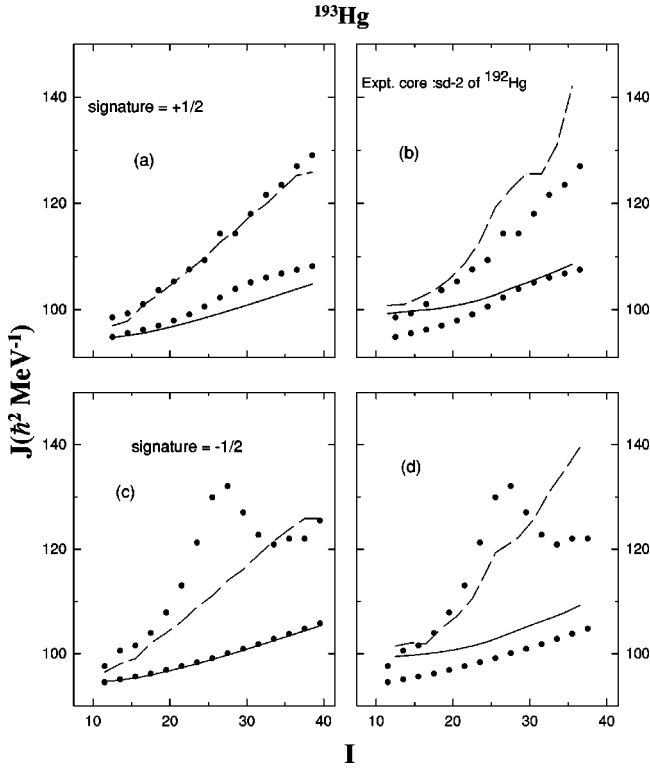
FIG. 2. (a), (b), (c), and (d) Comparison between theoretical and experimental kinematic and dynamic moments of inertia $\mathfrak{J}^{(1)}$ and $\mathfrak{J}^{(2)}$ for (a) and (b) $+1/2$ signature states, (c) and (d) $-1/2$ signature states of ^{193}Hg for two different choices of cores. The experimental data are marked by symbols. The corresponding theoretical points are joined by lines, continuous for $\mathfrak{J}^{(1)}$ and dashed for $\mathfrak{J}^{(2)}$.

FIG. 3. (a), (b), (c), and (d) Comparison between theoretical and experimental transition energies and dynamic moments of inertia (E_γ and $\mathfrak{J}^{(2)}$) for (a) and (b) SD-1 states, (c) and (d) SD-2 states of ^{191}Hg. The corresponding quantities for bands (a) and (b) [16] together in ^{195}Hg are shown in (e) and (f). (g) Comparison between theoretical and experimental kinematic moment of inertia for ^{195}Hg. The experimental data are marked by symbols. The corresponding theoretical points are joined by lines (the detailed description of the lines are in Table VI).

$A=150$ region is almost constant (Fig. 4). The detailed decomposition of the wave functions obtained from the present calculation of the superdeformed states in these two mass regions is shown in Table V. In this table, results for two representative nuclei in the two regions are chosen. They are ^{155}Dy and ^{193}Hg. The two columns in the table correspond to two different values of $\delta=0.30$ (normal deformation, corresponding to a hypothetical normal deformed state) and 0.570 or 0.475 (corresponding to the superdeformed state). Table VI shows other relevant parameters used for this calculation.

1. ^{155}Dy

Table V A shows the results for ^{155}Dy, a representative of the $A=150$ region. Part I of the table shows the decomposition of the wave function of the Nilsson 1/2[660] orbital, which is the Fermi level for this nucleus. The percentage amplitude of different j states ($|C_{jK}|^2$) [Eq. (5)] are shown in this part for two different values of deformation. For $\delta=0.30$, this $\chi_{K=1/2}$ states shows a 76% contribution from the high-$j=i_{13/2}$ state. As a result, $\langle J^2 \rangle$ ($=42.40$) and $\langle J \rangle$ ($=5.9$) also show a deviation from the value 48.75 and 6.5 expected for a pure $i_{13/2}$ composition. But for the superdeformed state $\delta=0.57$, this Nilsson state loses its high-j($=13/2$) composition. It is now a strong mixture of $i_{13/2}$ (36%), $g_{9/2}$ (36%),

and $d_{5/2}$ (18%). Part II of this table gives the $|f_{IK}|^2$ [Eq. (7)], i.e., the percentage Coriolis mixing amplitude of different bands (denoted by the Nilsson quantum numbers of the band heads) in the eigenfunction of the lowest energy final state of $I=40.5$. As expected, the state with smaller deformation shows a stronger Coriolis mixing, whereas the SD state with a larger value of the moment of inertia (smaller strength of Coriolis interaction, see also discussion on pairing gap in Sec. II B) and larger energy spacings among the quasiparticle states, has an 85% contribution from the band based on 1/2[660]. It is well known that, for a nucleus with Fermi level (λ) near the low-K states of a high-j orbital, the rotational band built on this orbital shows a "decoupled" structure. Instead of having **I** as vectorial sum of **R** and **j**, the total angular momentum I is just an algebraic sum of R and j, i.e., the rotational compositions of the final states are sharp compared to the states of a normal rotational band of an odd-A nucleus. So it is seen that the "decoupled structure" is more prominent for the normally deformed state as it has a sharper R composition, 71% from $R=34$ (as $I=40.5=34.0+6.5$). For the SD state, the decoupled structure is disturbed and $R=34,36,38,40$ are strongly mixed with 28%, 34%, 23%, and 10%, respectively, similar to the strong mixing between the j states 13/2, 9/2, and 5/2 in the intrinsic structure.
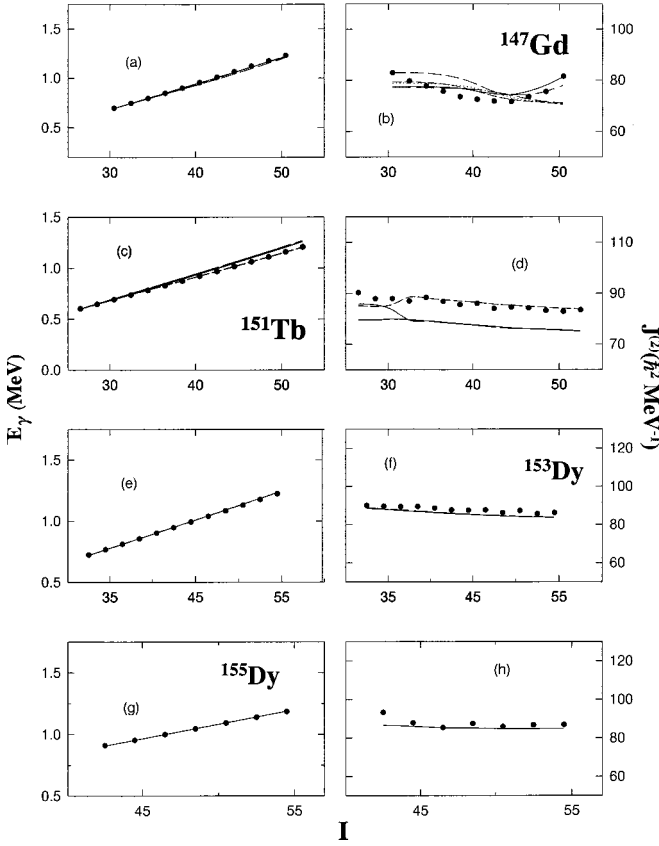
FIG. 4. Comparison between theoretical and experimental transition energies and dynamic moments of inertia (E_γ and $\mathfrak{I}^{(2)}$) for the SD bands of (a) and (b) ^{147}Gd, SD-1 (c) and (d) ^{151}Tb, SD-2 (e) and (f) ^{153}Dy, SD-1, and (g) and (h) ^{155}Dy, SD-1.

2. ^{193}Hg

For the $A=190$ region, the representative nucleus chosen is ^{193}Hg. Table V B shows the results for ^{193}Hg. Part I of the table shows the decomposition of the Nilsson 7/2[743] orbital, which is nearest to the Fermi level for this nucleus. The percentage amplitude of different j states ($|C_{jK}|^2$) [Eq. (5)] are shown in part for two different values of deformation. For $\delta=0.30$, this $\chi_{K=7/2}$ state shows a 90% contribution from the high-$j=j_{15/2}$ state. As a result, $\langle J^2 \rangle$ ($=61.06$) and $\langle J \rangle$ ($=7.3$) also show a small deviation from the value 63.75 and 7.5 expected for a pure $j_{15/2}$ composition. But for the SD configuration, $\delta=0.475$, this Nilsson state has a relatively (w.r.t $\delta=0.30$ state) reduced (82%) contribution from the high-j ($=15/2$) orbital. This is in direct contrast with the structure for the ^{155}Dy 1/2[660] state, which is strongly mixed. In Part II of this table, the final state, $I=9.5$ is expressed in terms of the percentage Coriolis mixing amplitudes [Eq. (7)]. As expected, the state with smaller deformation shows a stronger Coriolis mixing, whereas the superdeformed state has 98% contribution from the band based on 7/2[743]. In comparison with the ^{155}Dy SD state (λ near $K=0.5$), the Coriolis mixing is weaker here due to the proximity of a higher K ($=7/2$) Nilsson orbital to the Fermi level. Finally, in Part III of the table, the normally deformed state shows a good admixture of different R values (R

$=2,6,8,12$ with 31%, 33%, 12%, 13% contribution), as expected from the proximity of the $K=7/2$ near the Fermi level. As for ^{155}Dy, the SD state here also shows a stronger mixture of different R states ($R=2,6,8,12,14,16$, with 17%, 16%, 19%, 15%, 17%, and 10% contribution).

3. Cause of variation of $\mathfrak{I}^{(2)}$ in two mass regions

The above decomposition of the wave functions of the final states in the SD bands of ^{155}Dy and ^{193}Hg in terms of single-particle good j states and good R (core) states has given some information about the differences in the behavior of the dynamical moment of inertia in these two regions. In ^{155}Dy, the intrinsic state involved has a very strong admixture of different j values, with the high-j ($=13/2$) state having only a 36% contribution. Therefore, for this nucleus (or similar ones in $A=150$, where deformation values are similar, $\delta=0.57$, and Fermi levels are near low-K states) high-j alignment is not favorable. The dynamical moment of inertia is also nearly constant with a small variation due to the Coriolis antipairing effect (CAP), where the observed change is due to the weakening of pairing correlation between many orbitals (not necessarily the high-j ones) due to the Coriolis force. But for ^{193}Hg ($A=190$ region), deformation is comparatively smaller ($\delta=0.475$) and, therefore, the intrinsic structure has a higher contribution (82%) from the high-j state (which is also larger in this mass region, $j=15/2$). Although the Fermi level lies near the higher K states, involvement of the high-j orbitals favors alignment effect better and CAP effect also contributes. This results in a much stronger variation in the dynamical moment of inertia with spin.

B. Results of calculation of specific SD bands in $A=150$ and 190

The band structures in a few odd-proton and odd-neutron superdeformed nuclei in the $A=150$ and 190 regions have been calculated in the present work. Usually, only SD-1 bands have been calculated using SD-1 band of the corresponding core, unless mentioned otherwise. Dynamical and kinematic moments of inertia are also calculated for each band. Electromagnetic properties have also been determined in a few cases. Calculations are done in $^{193,195}_{81}$Tl, $^{191,193,195}_{80}$Hg, $^{153,155}_{66}$Dy, $^{151}_{65}$Tb, and $^{147}_{64}$Gd. We have plotted the experimental quantities as discrete symbols and joined the various theoretical results (corresponding to different choices of parameters) by different types of lines. Table VI contains a detailed list of such combinations. The comparison between calculated and experimental transition energies and moments of inertia are presented through a series of plots (Figs. 1–4). Instead of discussing results of individual nucleus, the gross features of total results have been discussed in the following paragraphs.

(i) For ^{193}Tl, Chen and Xing [4] quoted that energy r.m.s. deviation, defined as

$$\sigma = \sqrt{\frac{1}{n} \sum_I |E_\gamma(\text{calc},I) - E_\gamma(\text{exp},I)|^2}. \qquad (13)$$

TABLE V. Composition of the $I=$(A) 40.5 state of ^{155}Dy, (B) 9.5 state of ^{193}Hg. See text for detail.

State $K[N\Lambda\Sigma]$	j	$|C_{jK}|^2$(%) $\delta=0.30$	$\delta=0.57$	State $K[N\Lambda\Sigma]$	j	$|C_{jK}|^2$(%) $\delta=0.30$	$\delta=0.475$
					7.50	90.19	81.70
0.5[660]	6.50	75.87	35.64	3.5[743]	6.50	0.72	1.82
	5.50	0.08	0.93		5.50	8.84	15.60
	4.50	20.58	36.32		4.50	0.11	0.43
A.I. ^{155}Dy	3.50	0.10	2.39	B.I. ^{193}Hg	3.50	0.14	0.44
	2.50	3.04	17.99				
	1.50	0.09	2.89				
	.50	0.24	3.82				
$\langle J^2\rangle$		42.40	28.79			61.05	58.73
$\langle J\rangle$		5.94	4.60			7.31	7.14

State (I)	$K[N\Lambda\Sigma]$	$|f_{IK}|^2$(%) $\delta=0.30$	$\delta=0.57$	State (I)	$K[N\Lambda\Sigma]$	$|f_{IK}|^2$(%) $\delta=0.30$	$\delta=0.475$
40.5	0.5[660]	59.56	85.45	9.5	0.5[770]	0.0	0.0
	1.5[651]	31.87	13.77		1.5[761]	0.01	0.0
	2.5[642]	7.70	0.76		2.5[752]	1.16	0.61
A.II. ^{155}Dy	3.5[633]	0.82	0.02	B.II. ^{193}Hg	3.5[743]	49.68	98.46
	4.5[624]	0.04	0.0		4.5[734]	48.75	0.93
	5.5[615]	0.0	0.0		5.5[725]	0.39	0.0
	6.5[606]	0.0	0.0		6.5[716]	0.0	0.0
					7.5[707]	0.0	0.0

State (I)	R	$|C_R|^2$(%) $\delta=0.30$	$\delta=0.57$	State (I)	R	$|C_R|^2$(%) $\delta=0.30$	$\delta=0.475$
40.5	34	70.72	28.07	9.5	2	31.07	16.80
	36	24.32	34.41		4	5.84	3.46
	38	4.39	22.60		6	32.78	16.04
	40	0.51	10.35		8	12.01	19.26
A.III. ^{155}Dy	42	0.04	3.55	B.III. ^{193}Hg	10	3.98	1.92
	44	0.01	0.89		12	13.18	14.69
	46	0.0	0.13		14	0.26	17.34
					16	0.86	10.49
$\langle R\rangle$		34.70	36.60			5.94	9.04

is 1.2 keV for 26 states for both signatures together, with a small value of $\gamma=4.5°$. For $\gamma=0.0, \sigma=0.5$ keV for $+1/2$ signature and $\sigma=5.9$ keV for $-1/2$ signature. In our calculation, with an experimental core the modified σ values are (with $\gamma=0.0$), $\sigma=0.56$ keV for $+1/2$ signature and $\sigma=2.96$ keV for $-1/2$ signature. For both the signatures together the deviation is 2.13 keV [Figs. 1(a) and 1(b)]. So in our calculation, with an experimental core the need of inclusion of the triaxiality parameter is much less compared to the previous calculations. This is obvious from the difference in deviations for the two signature sets. The signature dependence of the deviation is an indicator of the γ deformation. So still there exists an indication of a small triaxiality, whereas, for ^{195}Hg, both the signature shows equal good fits [Figs. 3(e)–3(g)], indicating $\gamma=0.0$.

(ii) As a general observation it must be noted that the dynamic moment of inertia is a better quantity to identify the best set of parameters. It is seen that different sets of parameters may not show much difference in the corresponding values of E_γ's, but the dynamic moments of inertia when plotted clearly differentiate between the different choices, e.g., as shown in Fig. 4, in ^{147}Gd and ^{151}Tb.

(iii) The single-particle states included in the calculations originate from the intruder orbitals of the relevant shells in the corresponding mass regions. But the spins and parities of these superdeformed bands are not unambiguously assigned. It can be seen that the states originating from any one of the two intruder states from the two consecutive opposite parity shells can give nearly similar agreement to the experimental spectrum. These two states generate favored states of two opposite signatures and different parities which can be accommodated within the error in the spin determination of the

TABLE VI. Different parameter values (pairing gap Δ is in MeV) used for calculations of different SD bands in various isotopes. The symbols have their usual meanings, as discussed in Sec. II. A indicates normal Δ, reduced α; B indicates reduced Δ, normal α; C indicates normal Δ, normal α; D indicates reduced Δ, reduced α.

Isotope	μ	κ	δ	Δ	λ_n/λ_p	State	α	Core	Figure	Comment
^{193}Tl	0.6183	0.0616	0.475	0.985	46.20	5/2[642]	0.58	^{192}Hg	1(a),1(b)	A
				0.250			0.76			B
^{195}Tl	0.6196	0.0614	0.475	0.957	46.30	>5/2[642]	0.50	^{194}Hg	1(c)–1(e)	A
^{191}Hg	0.3883	0.0636	0.475	1.1	52.00	5/2[752]	0.94	^{190}Hg	3(a),3(b) (solid)	C
(SD-1)				0.3	48.96	1/2[770]	0.84	^{190}Hg	(long dash)	B
^{191}Hg	0.3883	0.0636	0.475	1.1	52.00	5/2[752]	0.42	^{192}Hg	3(c),3(d) (solid)	A
SD-2					47.20	5/2[642]	0.55	^{192}Hg	(long dash)	A
^{193}Hg	0.3858	0.0636	0.475	0.9	55.00	>7/2[743]	0.475	^{192}Hg (SD-1)	2(a)–2(d)	A
^{193}Hg				0.96	54.00	<7/2[743]	0.40	^{192}Hg (SD-2)		A
^{195}Hg	0.3834	0.0636	0.475	1.05	52.5	9/2[624]	0.69	^{194}Hg	3(e)–3(g) (solid)	A
^{155}Dy	0.4327	0.0637	0.57	1.26	46.67	1/2[660]	0.975	^{154}Dy	4(g),4(h) (solid)	C
^{153}Dy	0.4352	0.0637	0.57	0.50	46.90	1/2[660]	0.45	^{152}Dy	4(e),4(f) (long dash)	D
				1.10	53.00	1/2[770]	0.55		(solid)	A
^{151}Tb	0.5910	0.0648	0.57	1.50	52.62	1/2[770]	0.29	^{152}Dy	4(c),4(d) (short dash)	A
(SD-2)					47.07	1/2[660]	0.15	^{150}Tb [a]	(solid)	A
							0.57	^{150}Tb [b]	(long dash)	A
					52.62	1/2[770]	0.615	^{150}Tb [b]	(med. dash)	A
^{147}Gd	0.4426	0.0637	0.57	1.20	47.52	1/2[660]	0.96	^{146}Gd [b] (SD-1)	4(a),4(b) (solid)	C
					53.40	1/2[770]	0.56		(long dash)	A
					53.40	1/2[770]	0.06	^{146}Gd [a] (SD-2)	(med dash)	B
					47.52	1/2[660]	0.80	^{146}Gd [b] (SD-2)	(short dash)	C
					53.40	1/2[770]	0.44	^{146}Gd [b] (SD-2)	(dot)	A

[a]NDS (Nuclear Data Sheets) spin [1].
[b]Spin predicted by Eq. (11).

SD bands [Table VI, ^{191}Hg in Figs. 3(a)–3(d) and ^{151}Tb and ^{147}Gd in Fig. 4].

(iv) The effect of the choice of different SD core is evident from Fig. 2. It can be clearly seen that the final results are extremely sensitive to the core chosen. The even-even core may possess more than one SD band, it is always very important to choose the proper SD band of the core corresponding to that particular SD band of the odd-A nucleus, to have a good agreement. For example, for ^{193}Hg, the dynamical moments of inertia clearly show a big difference for two choices of the ^{192}Hg core. Similar strong core dependence is manifested in the calculations for ^{151}Tb and ^{147}Gd also. For ^{151}Tb, SD-2, the ^{152}Dy SD-1 core is definitely a better choice than the ^{150}Tb, SD-1. Similarly for ^{147}Gd, the ^{146}Gd, SD-1 band is the proper core (Table VI, Figs. 2 and 4). It is found that for most odd-A lowest SD bands, the lowest SD band in the core is the most appropriate except for ^{151}Tb and ^{193}Hg. This contradicts the expectation that due to a generic simplicity of the SD bands, the input of any SD core almost guarantees a correct result in odd neighbors without any coupling or calculations.

(v) The reduction in pairing in the superdeformed bands as observed in the earlier studies is also evident from the present calculation. This is manifested through a comparatively larger attenuation of the Coriolis matrix elements as discussed before. Moreover, as superdeformed cores are used in this calculation, the effect of reduced pairing is already

incorporated in the experimental core spectrum. So in some cases, e.g., in ^{191}Hg additional reduction may not be necessary (attenuation $\alpha = 0.94$, usual value).

(vi) The $B(M1)$ values calculated for ^{195}Tl show an appreciable signature dependence (Fig. 1). But it is not so strong as observed in the calculations of Xing et al. [6]. The signature averaged value of $B(M1)$ from the present calculation comes out to be 0.65 μ_N^2 consistent with the calculated $B(M1)$ value in [25].

(vii) The calculations in ^{195}Hg need special mention. In a recent experiment [16] four new SD bands have been identified in this isotope of Hg. The minimum spins have also been assigned by the previous workers tentatively. We have used those values of spins and calculated E_γ, $\mathfrak{J}^{(1)}$, $\mathfrak{J}^{(2)}$ for the lowest two SD bands. We have plotted both the signatures together and the results show that the two signatures are in excellent agreement with the two SD bands as reported earlier. It is, therefore, very obvious that these two bands are signature partners.

(viii) Finally, the underlying assumption in this model is that, even in the presence of an unpaired nucleon, the excitation energies of the core remain the same [13], the possible polarizing effects of the last unpaired nucleon is neglected. However, even if the core remains unperturbed in the presence of an unpaired valence nucleon, the experimental bands in the odd- and even-A neighbors, in general, will not show identical moments of inertia because of band mixing due to

the Coriolis interaction. The success of the application of this model in the superdeformed region shows that the inclusion of an odd particle to the superdeformed core does not disturb its structure.

IV. CONCLUSION

The present calculation shows that the simple version of PRM with the experimental core energies as the input is quite capable of explaining the superdeformed bands in the odd-A nuclei in the $A = 150$ and 190 regions. This simple model can be very easily applied to the other regimes of superdeformation in other mass regions. The present calculation also shows that different trends of $\mathfrak{I}^{(2)}$ in the two mass regions manifest the difference in the extent of involvement of the high-j orbitals in their intrinsic structure.

[1] B. Singh, R. B. Firestone, and S. Y. F. Chu, Nucl. Data Sheets **78**, 1 (1996); X. Han and C. Wu, At. Data Nucl. Data Tables **63**, 117 (1996).

[2] P. J. Nolan and P. J. Twin, Annu. Rev. Nucl. Part. Sci. **38**, 533 (1988).

[3] B. M. Nyako *et al.*, Phys. Rev. Lett. **52**, 507 (1984).

[4] X. Q. Chen and Z. Xing, J. Phys. G **19**, 1869 (1993).

[5] X. Q. Chen and Z. Xing, J. Phys. G **20**, 1041 (1994).

[6] Z. Xing and X. Q. Chen, J. Phys. G **22**, 1343 (1996).

[7] J. Terasaki, P. H. Heenen, P. Bonche, J. Dobaczewski, and H. Flocard, Nucl. Phys. **A593**, 1 (1995).

[8] S. Zhou and C. Zheng, Phys. Rev. C **55**, 2324 (1997); S. Zhou, C. Zheng, F. Xu, and J. Hu, Nucl. Phys. **A615**, 229 (1997).

[9] A. K. Jain, M. Dudeja, S. S. Malik, and Z. Ahmed, Phys. Lett. B **392**, 243 (1997).

[10] E. M. Müller and U. Mosel, J. Phys. G **10**, 1523 (1984).

[11] M. Saha, A. Goswami, S. Bhattacharya, and S. Sen, Z. Phys. A **332**, 383 (1989).

[12] M. Saha, A. Goswami, S. Bhattacharya, and S. Sen, Phys. Rev. C **42**, 1386 (1990).

[13] A. Mukherjee, U. Datta Pramanik, M. (Saha) Sarkar, and S. Sen, Phys. Rev. C **50**, 1868 (1994).

[14] S. Bhattacharya, S. Sen, and R. K. Guchhait, Phys. Rev. C **32**, 1026 (1985).

[15] A. Goswami, S. Bhattacharya, M. Saha, and S. Sen, Phys. Rev. C **37**, 370 (1988).

[16] G. Hackman *et al.*, Phys. Rev. C **55**, 148 (1997).

[17] S. M. Fischer *et al.*, Phys. Rev. C **54**, R2806 (1996).

[18] Ch. Theisen *et al.*, Phys. Rev. C **54**, 2910 (1996).

[19] K. Neergärd, Phys. Lett. **89B**, 5 (1979).

[20] H. A. Smith, Jr. and F. A. Rickey, Phys. Rev. C **14**, 1946 (1976).

[21] S. G. Nilsson, C. F. Tsang, A. Sobiczewski, Z. Szymanski, S. Wycech, C. Gustafson, I. L. Lamm, P. Moller, and B. Nilsson, Nucl. Phys. **A131**, 1 (1969).

[22] G. Audi and A. H. Wapstra, Nucl. Phys. **A565**, 1 (1993).

[23] R. V. F. Janssens and T. L. Khoo, Annu. Rev. Nucl. Part. Sci. **41**, 321 (1991).

[24] J. Duprat *et al.*, Phys. Lett. B **341**, 6 (1994).

[25] P. B. Semmes, I. Ragnarsson, and S. Åberg, Phys. Lett. B **345**, 185 (1995).